FEMS Microbes, 2024, 5, xtae018
DOI: 10.1093/femsmc/xtae018
Advance access publication date: 3 June 2024
Research Article – Microbes & Metabolism

The role of the universal sugar transport system components PtsI (EI) and PtsH (HPr) in *Enterococcus faecium*

Michelle Hallenbeck[1,2], Michelle Chua[1,2], James Collins [1,2,3,*]

[1]Department of Microbiology & Immunology, University of Louisville, Louisville, KY 40202, United States
[2]Center for Predictive Medicine, University of Louisville, Louisville, KY 40202, United States
[3]Center for Microbiomics, Inflammation and Pathogenicity, University of Louisville, Louisville, KY 40202, United States
*Corresponding author. Department of Microbiology & Immunology, University of Louisville, Louisville, KY 40202, United States. E-mail: james.collins.1@louisville.edu
Editor: [Kathleen Scott]

Abstract

Vancomycin-resistant enterococci (VRE) pose a serious threat to public health because of their limited treatment options. Therefore, there is an increasing need to identify novel targets to develop new drugs. Here, we examined the roles of the universal PTS components, PtsI and PtsH, in *Enterococcus faecium* to determine their roles in carbon metabolism, biofilm formation, stress response, and the ability to compete in the gastrointestinal tract. Clean deletion of *ptsHI* resulted in a significant reduction in the ability to import and metabolize simple sugars, attenuated growth rate, reduced biofilm formation, and decreased competitive fitness both *in vitro* and *in vivo*. However, no significant difference in stress survival was observed when compared with the wild type. These results suggest that targeting universal or specific PTS may provide a novel treatment strategy by reducing the fitness of *E. faecium*.

Keywords: Biofilm; *Enterococcus faecium*; Sugar metabolism; PTS; ptsIH; VRE

Introduction

Enterococcus faecium, a common commensal bacterium in the lower gastrointestinal tract of humans and animals, has emerged as an opportunistic pathogen causing life-threatening hospital-associated infections. The global prevalence of vancomycin-resistant enterococci (VRE) has increased since their emergence in the 1980 s, with approximately 75% of clinical *E. faecium* isolates exhibiting vancomycin resistance (Gilmore et al. 2013). This trend poses a therapeutic challenge, as *E. faecium* isolates commonly possess both intrinsic and acquired resistance to antibiotics, including "last-line-of-defense" options, such as linezolid and daptomycin (Fiore et al. 2019, Turner et al. 2021).

Previous studies have revealed a correlation between increased sugar availability and the expansion of clinical *E. faecium* (Zhang et al. 2013, Stein-Thoeringer et al. 2019, Fajstova et al. 2020, Khan et al. 2020, Wang et al. 2020). Furthermore, clinical *E. faecium* strains are enriched in sugar transport and metabolism genes compared to commensal strains (Lebreton et al. 2013, Gao et al. 2018). Three types of sugar transport systems are found in bacteria: phosphoenolpyruvate: sugar phosphotransferase system (PTS), electrochemical cation-gradient-driven symporters, and binding protein-dependent adenosine triphosphate-binding cassette (ABC) import systems. The predominant sugar transporters annotated in Enterococci are the Phosphotransferase systems (PTS) that detect, transport, and phosphorylate monosaccharides, disaccharides, amino sugars, polyols, and other sugar derivatives (Deutscher et al. 2006). This system comprises multiple proteins, including two general proteins, PtsI (Enzyme I or EI) and the Histidine-containing Phosphocarrier Protein, PtsH (HPr), which are utilized for all sugars. Additionally, specific transporters for each sugar or sugar group provide specificity (Fig. 1A).

PTS not only function as carbohydrate transporters, but also regulate numerous cellular processes either by phosphorylating their target proteins or by interacting with them in a phosphorylation-dependent manner (Galinier and Deutscher 2017). Sugar-specific PTS or the universal enzymes PtsI and PtsH have been demonstrated to be involved in regulatory processes involving carbon through carbon catabolite repression (CCR), both independently and as a co-repressor with the catabolite control protein (CcpA). A role in nitrogen, and phosphate metabolism; chemotaxis; potassium transport; cold shock response; hydrogen peroxide resistance; biofilm formation; and virulence has also been demonstrated in multiple species (Graumann et al. 1996, Kok et al. 2003, Phadtare 2004, Beaufils et al. 2007, Monedero et al. 2007, Houot and Watnick 2008, Houot et al. 2010a,b, Le Bouguenec and Schouler 2011, Zhang et al. 2013, Gera et al. 2014, Derkaoui et al. 2016, Paganelli et al. 2016, Peng et al. 2017, Gao et al. 2018, Horng et al. 2018, Bier et al. 2020, Liao et al. 2022).

In this study, we investigated the roles of the universal sugar transport system components, PtsH and PtsI, to better understand how they contribute to these processes in *E. faecium* and assess their potential as future exploratory targets for the development of novel therapeutics.

Received 13 March 2024; **revised** 8 May 2024; **accepted** 31 May 2024

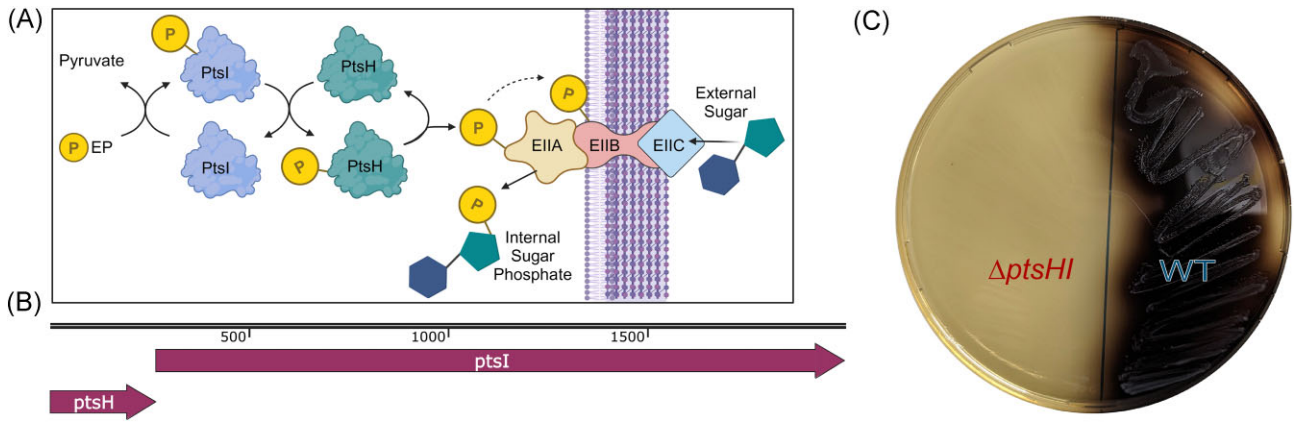

Figure 1. PTS in *E. faecium*. (A) Constituents of typical PTS permeases. The sugar substrate is delivered through the membrane from the extracellular medium via a pathway defined by the integral membrane permease-like Enzyme IIC. Energy-coupling proteins transmit a phosphoryl group from the initial phosphoryl donor, phosphoenolpyruvate (PEP), via PtsI (Enzyme I), PtsH (HPr), Enzyme IIA, and Enzyme IIB to the final phosphoryl acceptor, sugar, resulting in sugar phosphate. (B) The *ptsHI* operon of *E. faecium*. (C) Wildtype and Δ*ptsHI* strains cultured on Bile Esculin Agar (BEA). The WT produces black pigmentation due to its ability to import (via PTS) and hydrolyze esculin to glucose and esculetin, which reacts with ferric ions to form a black precipitate.

Materials and methods

Bacterial growth conditions

All bacterial strains were stored in 10% DMSO stocks at −70°C. Bacterial cultures were routinely grown at 37°C on Brain Heart Infusion (BHI) agar or in BHI medium with shaking. To assess growth on single carbon sources, a carbon source limited medium (M1) was prepared, as reported by Zhang *et al.* (Zhang et al. 2011). To assess growth in rich media, wild-type and Δ*ptsHI* strains were propagated for ∼9 h in BHI, diluted back to an OD_{600} of 0.1 in BHI without glucose, and further diluted 1:10 into either standard BHI which contains 0.2% w/v glucose or BHI without any added sugar.

Generation of the Δ*ptsHI* mutant

A CRISPR-Cas12 system was used to generate clean deletion mutants of *ptsHI* in *E. faecium* NCTC7171 as previously described (Chua and Collins 2022). Briefly, three inserts, a small RNA promoter driving the CRISPR protospacer RNA, and up- and downstream arms homologous to the flanking regions surrounding the *ptsHI* were amplified by PCR with primers containing splicing by overlap extension (SOE) PCR-compatible overhang regions (5′-AAAAAGATGCCAGTGTGCTG-3′ and 5′-AATTACATCAGAACCTTGACCTACACCATCTACAAGAGTAGAAATTATGGTGGAATGATAAGGGTT-3′; 5′-GTCAAGGTTCTGATGTAATTTCTACTCTTGTAGATTCGTTGCCTCATTCTTGCCG-3′ and 5′-AGTTCAACGACTTCTTCTACTAATAGTGTAGCTGGACGAGCG-3′; and 5′-CCAGCTACACTATTAGTAGAAGAAGTCGTTGAACTTGTTCATGA-3′ and 5′-GCATGTCTGCAGGCCTCGAGCGGCACACGGATACCATAGC-3′, respectively). Fifty nanograms of the largest fragment and equimolar amounts of the smaller pieces were combined into a 20-µL final volume of Q5 PCR master mix without primers and cycled under the following conditions: 98°C for 10 s, 10 cycles of 98°C for 10 s, 57°C for 30 s, and 72°C for 50 s, followed by 72°C for 10 min. After the first round of SOE PCR, 1 µL of each universal SOE primers (5′-GAGAAATCCCTAAATAAAAAGATGCCAGTGTGCTG-3′ and 5′-GCCAGTGCCAAGCTTGCATGTCTGCAGGCCTCGAG-3′) was added, and the reaction mixture was returned to the thermocycler at 98°C for 2 min, 15 cycles of 98°C for 10 s, 65°C for 30 s, and 72°C for 50 s, followed by 72°C for 10 min. The SOE PCR product was analyzed on a 1% agarose gel to confirm a single band of the correct size. The plasmid backbone pJC005.gent was linearized by PCR (primer pair oJC218-oJC219), and template DNA was removed via DpnI digestion. Fifty nanograms of linearized plasmid backbone and 1 µl of SOE PCR product were mixed and directly transformed into chemically competent *E. coli* DB10 cells for *in vivo* cloning. Colonies were checked 24 h later for the correct insert by colony PCR, and the correct full plasmid sequence was confirmed by whole plasmid sequencing (Plasmidsaurus).

The *PtsHI* knockout plasmid was electrotransformed into *E. faecium* NCTC7171, and a single colony was struck on BHI agar supplemented with 125 µg mL^{-1} gentamicin and 200 ng mL^{-1} ahTC and incubated at 37°C. Twenty colonies were randomly selected for colony PCR to screen for mutants. The correct deletion was confirmed in 100% of the screened colonies. The Cas12a plasmid was cured by streaking a colony with the desired deletion onto BHI agar plus 200 ng mL^{-1} ahTC without antibiotics and incubating it overnight. Following growth, the colonies were patch-plated with and without gentamicin to confirm plasmid loss.

ptsHI complementation

To complement the *ptsHI* operon back into *E. faecium* NCTC7171Δ*ptsHI*, a plasmid containing the *ptsHI* operon driven by the *tetR* promoter was used. The plasmid backbone containing *tetR* (pJC007) was linearized by PCR using primers 5′-GAATATGTAAAATAATATGACCATGATTACGAATTCGAGC-3′ and 5′-TTCTTTCTTTTCCATAAAAACCTCCTTTACTGCAGGAG-3′. The resulting product was digested with DpnI to remove template DNA. The *ptsHI* operon were amplified using primer pair 5′-GTTTTTATGGAAAAGAAAGAATTTCACGT-3′ and 5′-TCATATTATTTTACATATTCATGAACAAGTTCA-3′ from *E. faecium* NCTC7171 genomic DNA. One microliter of the backbone and insert were mixed and transformed into *E. coli* DB10 for *in vivo* cloning. Colonies were checked 24 h later for the correct insert by colony PCR and confirmed by full plasmid sequencing. The sequenced plasmid was electroporated into NCTC7171Δ*ptsHI* cells to generate NCTC7171Δ*ptsHI*:: *ptsHI*.

Determination of PTS-dependent sugars by growth on single carbon sources

Wild-type and Δ*ptsHI* strains were grown overnight in BHI, diluted back to an OD_{600} of 0.01 in M1 media, and inoculated into Biolog

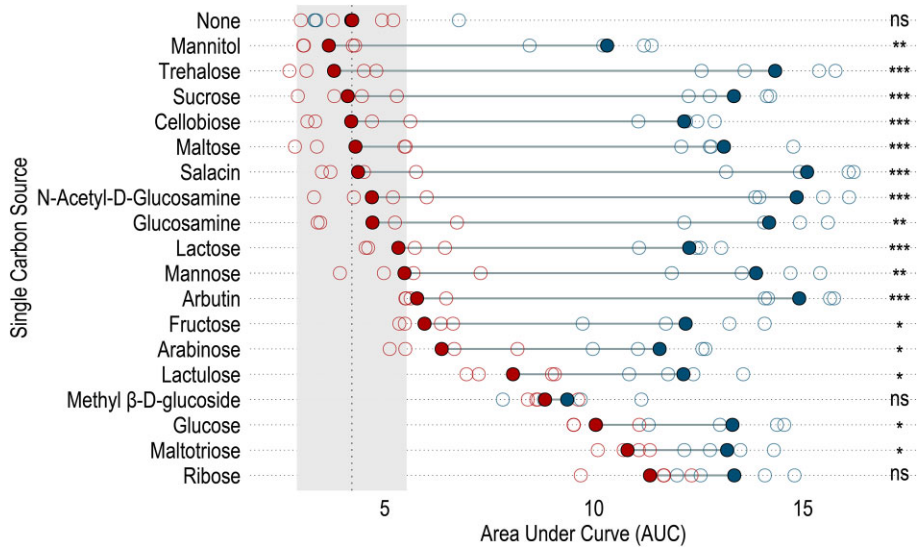

Figure 2. Most metabolizable sugars in *E. faecium* are transported via PTS. The WT and Δ*ptsIH* strains were grown in M1 medium supplemented with 0.5% w/v of a single carbon source. Growth was tracked using a microplate reader and after 24 h, the area under the curve (AUC) was calculated. Open circles represent biological replicates and closed circles represent the mean AUC. Red and Blue indicate the Δ*ptsIH* and WT strains, respectively. The dotted vertical line and shaded area indicate the mean AUC and SD, respectively, for growth in M1 medium without any additional carbon source. Four independent biological replicates were used for each strain for each growth condition. Statistical differences between the strains for each carbon source were calculated using Welch's t-test with Holm's correction for multiple comparisons. * $P \leq 0.05$, ** $P \leq 0.01$, *** $P \leq 0.001$ after correction.

plates PM1, PM2, or M1 media containing 0.5% of the sugar to be tested. Plates were incubated statically at 37°C in Stratus plate readers (Cerillo) set to record the OD_{600} every 10 min for 24 h.

Analysis of Microbial Growth Assays (AMiGA)

Growth curves were analyzed in Python (v3.10.10) using analysis of microbial growth assays (AMiGA) software (https://github.com/firasmidani/amiga) (Midani et al. 2021). AMiGA performed Gaussian Process regression to fit the curves to the data and test the differential growth between the wild-type and mutant strains. The functional difference in OD_{600} (and its credible interval) between the wild-type and mutant strains was also computed in the autolysis assay. The first few time points of the bacterial growth curves typically exhibit a very low signal-to-noise ratio, which can bias the inference of several growth parameters. To minimize this bias, the first 10 data points were skipped prior to calculating growth rates and doubling times.

Biofilm formation assay

The assay was based on previously published protocols for *E. faecium* (Heikens et al. 2007, Lebreton et al. 2012, Paganelli et al. 2013). Wild-type and Δ*ptsHI E. faecium* NCTC7171 strains were cultured overnight in Tryptic Soy Broth (TSB) supplemented with 0.25% glucose. The following morning, the cultures were normalized to an OD_{600} of 0.05 and 10 µl of inoculum was added to 190 µL of TSB in each well of a 96-well plate. Cultures were incubated statically in a Cerillo plate reader to record OD_{600} every 10 min at 37°C for 24 h. After 24 h of growth, the culture supernatant was removed and the wells were gently washed with PBS to remove non-adherent cells. A 0.1% crystal violet solution (1/2 volume of the initial medium) was added to the wells, and the plate was gently rocked for 5–10 minutes. The wells were washed with PBS and rocked again for 5–10 minutes to remove excess crystal violet. PBS was aspirated, and the plate was allowed to dry. An equal volume of the initial medium (200 µL) of acetone/ethanol solution was added to resolubilize the crystal violet, and the optical density (OD_{550}) of the biofilm was measured. Biofilm quantification is reported as the ratio of biofilm to biomass (OD_{550}/OD_{600}).

Autolysis susceptibility assay

Based on previously used protocols for *E. faecium* (Lebreton et al. 2012, Paganelli et al. 2013), early stationary phase cultures of wild-type and Δ*ptsHI E. faecium* NCTC7171 were normalized to an OD_{600} of 1. One-hundred microliters of normalized culture was then added to the wells of a 96-well plate containing 100 µl of PBS or PBS + 0.2% Triton X-100 (final concentration 0.1%). The plates were incubated statically at 37°C for 24 h, with OD_{600} readings taken every 10 min.

Acid resistance and Copper toxicity assays

Overnight cultures of wild-type and Δ*ptsHI E. faecium* were normalized to an OD_{600} of 1. 96-well plates were prepared with 190 µl per well of either BHI adjusted to varying pH levels (7, 6.5, 6, 5.5, 5, 4.5, and 4) using 5 M HCl or varying concentrations of copper (0, 4, 8, 12, and 16 mM $CuSO_4$ pentahydrate, adapted from Menghani et al. (2022)). Ten microliters of each culture were inoculated into each well and the plate statically incubated in a Cerillo plate reader at 37°C for 24 h with OD_{600} readings every 10 min.

Estimation of LD50

Alterations in bacterial growth curves, such as changes in lag time, maximum optical density (OD), growth rate, and doubling time, among others, were observed upon the introduction of stress. To capture these phenotypic changes, the area under the curve (AUC) was used to fit dose-response models. Given the distinct growth phenotypes of the wild-type (WT) and mutant strains, even in the absence of exogenous stressors, the response (AUC) was normalized to the maximum percentage for each strain. Dose-response models were fitted using a four-parameter log-logistic function from the Analysis of Dose-Response Curves package in R (v4.3.1) (Ritz et al. 2015).

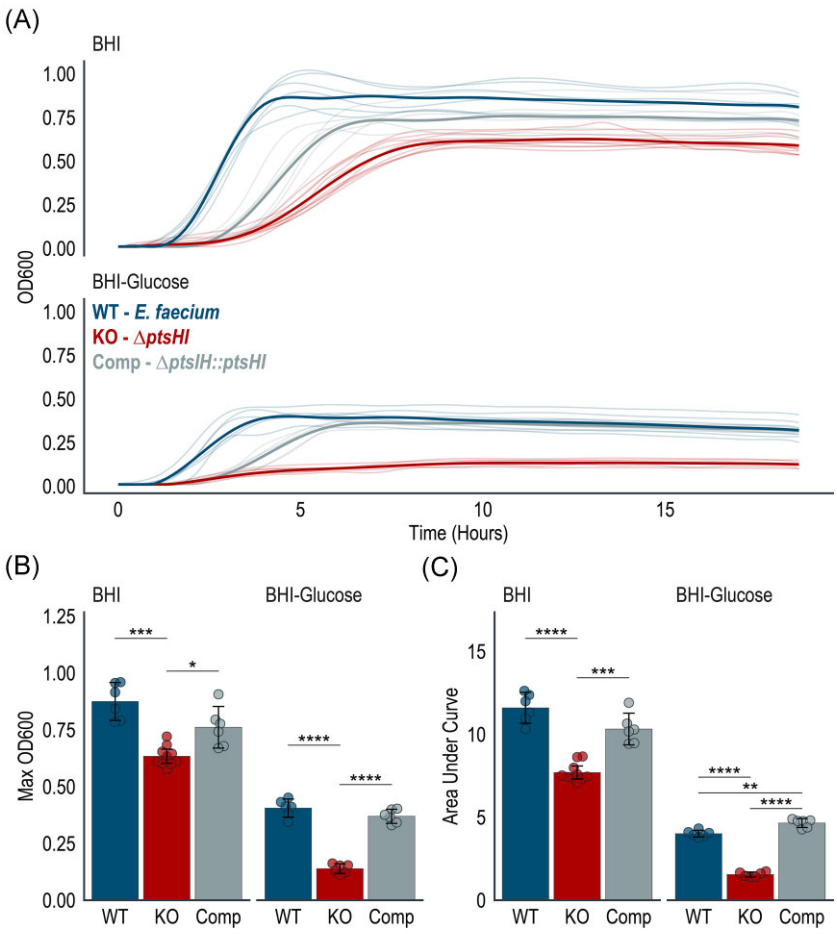

Figure 3. The Δ*ptsH I* mutant was significantly attenuated in rich media. A) Growth curves of the WT, Δ*ptsHI*, and complemented strains in BHI and BHI media without glucose. Thin lines indicate biological replicates and thick lines indicate Gaussian process (GP) regression curves generated from pooled replicate data. B) The Δ*ptsHI* (KO) strain had a significantly reduced maximum OD, which was restored upon complementation. C) The Δ*ptsHI* (KO) strain had a significantly reduced AUC, which was restored upon complementation. Eight independent biological replicates were used for each strain. Circles represent biological replicates; error bars are SD. Statistical differences between strains were calculated using Welch's t-test with Holm's correction for multiple comparisons. * $P \leq 0.05$, ** $P \leq 0.01$, *** $P \leq 0.001$ **** $P \leq 0.0001$ after correction.

Competitive fitness measurements

The relative fitness of the wild type and Δ*ptsHI* mutants was determined as described previously (Starikova et al. 2013). Briefly, five biological replicates of each strain were cultured overnight in BHI, adjusted to an OD_{600} of 1, and diluted 1:10 in pre-warmed BHI broth. Samples were serially diluted on BHI agar to confirm the initial cell density of each strain. Strains were further diluted and mixed by adding 100 µL of each strain to 2.8 mL of BHI. Following a 6-hour incubation period at 37°C with shaking (225 rpm), samples were diluted and plated onto Bile Esculin Agar (BEA) media to ascertain the final cell densities. While the WT strains produced colonies with black halos, the mutant strain produced smaller colonies that did not change color because of the inability to import esculin. The population growth, or Malthusian parameter (m), of each strain was calculated using the formula m = ln(N6/N0), where N6 and N0 represent the final and initial cell density, respectively. The relative fitness (w) was then determined as the ratio of the Malthusian parameters of the wild-type and Δ*ptsHI* mutant, given by $w = m_{wt}/m_{ptsHI}$. For *in vivo* competitive fitness, qPCR was used to determine *E. faecium* copy numbers (see below).

Mouse model

All procedures involving animals were reviewed and approved by the Institutional Animal Care and Use Committee of the University of Louisville (IACUC protocol number: 23 321). Gastrointestinal (GIT) colonization studies used 6-week-old female ICR mice (Envigo). Mice were screened for *E. faecium* after decolonization via qPCR using *E. faecium*-specific primers (Kim et al. 2022). The mice were decolonized as previously described (Montealegre et al. 2016). Briefly, four mice in the mono-inoculation assay and four mice in the competition assay were first decolonized for four days with 1 mg/mL gentamicin in drinking water plus subcutaneous injections of clindamycin (2.4 mg/day/mouse). Antibiotics were stopped 24 h prior to the gavage of bacteria, allowing for the elimination of the drug. NCTC7171Δ*ptsHI* was administered individually (for the mono-inoculation assay) or in a 1:1 combination with the WT strain (for the competition assay) in a suspension containing approximately 10^9 colony-forming units (CFUs). The number of CFUs was determined by plating serial dilutions of each inoculum in sterile PBS on BHI agar plates. Mouse stool was collected daily for six days, and *E. faecium* was quantified by qPCR.

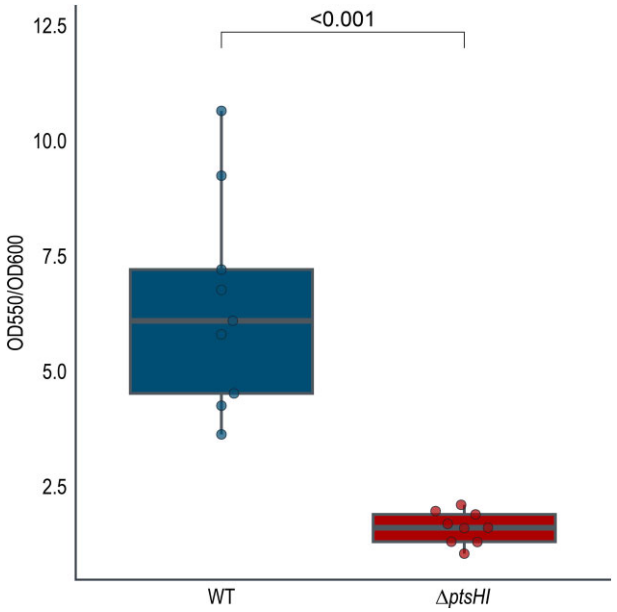

Figure 4. Biofilm production was significantly attenuated in Δ*ptsH I* strain. Biofilm formation was assessed using crystal violet staining (OD550) and normalized to the final OD600 value after 24 h of growth. Tukey box plot overlaid with biological replicates. Statistical differences between strains were calculated using Welch's t-test.

Quantification of *E. faecium* in stool by qPCR

To quantify the *E. faecium* burden in the murine mono-colonization and competition assays, we used a previously validated primer set to quantify total *E. faecium* (5′-ATATCGGCTGTCTCCATGCT-3′ and 5′-CCGCCGTCTATAATCCATTC-3′ (Kim et al. 2022), product length 121 bp, primer efficiency 96.16%) and a primer pair (5′-ACGTAGTAGCAGAAACTGGGATC-3′ and 5′-GCCACACCAGCTTTTGATACG-3′, product length 114 bp, primer efficiency 98.22%) to bridge the *ptsHI* deletion to detect the Δ*ptsHI* strain. DNA was extracted from mouse stool using the DNeasy PowerLyzer PowerSoil Kit (Qiagen), according to the manufacturer's instructions. To quantify the genome copy number, a five-point standard curve was generated using purified NCTC7171Δ*ptsHI* genomic DNA ranging from 300 000 to 30 genome copies. For unknown samples, 10 ng of total DNA was used per 20 µl qPCR reaction (qPCRBIO SyGreen Blue Mix Lo-ROX, PCR Biosystems). Samples were run in triplicate on a QuantStudio 7 device and analyzed using the Applied Biosystems qPCR Analysis Modules within the Thermo Fisher Cloud.

Statistical analysis

Statistical analyses using ANOVA, Welch's two-sided t-test, and two-sample Wilcoxon tests were carried out in R (v4.3.2). Multiple comparisons were controlled using the Holm correction (Holm 1979). Figures were generated in R (v4.3.2) using the Tidyverse set of packages (Wickham et al. 2019). Statistical differences in LD50 derived from dose-response curves were determined using the Analysis of Dose-Response Curves package in R (Ritz et al. 2015).

Results and discussion

Generation of Δ*ptsHI* mutant

The bacterial PTS facilitates the concurrent transport of sugar substrates across the bacterial membrane and subsequent phosphorylation (Fig. 1A). The *ptsHI* genes are generally located in the same operon, although their order differs among species, with *ptsH* being the first in *E. faecium* (Fig. 1B). The deletion of *ptsI*, *ptsH*, or both results in an inability to utilize sugars that are entirely dependent on PTS. Single *ptsH* mutants have demonstrated a leaky phenotype in other species, owing to adaptive mutations (Min and Seok 2022); therefore, we created a double *ptsHI* clean deletion mutant in *E. faecium* NCTC7171, NCTC7171Δ*ptsHI*. To validate the mutant phenotype, we grew it alongside the wild-type (WT) strain on Bile Esculin Agar. Enterococci can hydrolyze esculin (a coumarin glucoside) to glucose and esculetin, which reacts with ferric ions to form a black precipitate. However, to hydrolyze esculin, bacteria must first import it into the cell via an unidentified PTS system. The shutdown of all PTS via the *ptsHI* double mutant resulted in an esculin-negative phenotype (Fig. 1C). Clean deletions were confirmed by PCR and Sanger sequencing. To ensure that the observed phenotypes were not due to pleiotropic effects, we generated a complemented strain (NCTC7171Δ*ptsHI*:: *ptsHI*) by constructing a plasmid containing the *ptsHI* operon under the control of the tetracycline promoter and transforming it into NCTC7171Δ*ptsHI*.

Most *E. faecium* metabolizable sugars are PTS-dependent

To determine the range of carbon sources metabolizable by *E. faecium* NCTC7171, we utilized Biolog Phenotype MicroArray plates PM1 and PM2. Each well contained a unique carbon source or no carbon control, enabling rapid profiling of 190 carbon sources. Following the growth of three biological replicates, sugars with ≥ 2 × the maximum OD of the no-carbon control were considered to be metabolizable by *E. faecium*. To enable the use of known sugar concentrations and increase biological replication, further experiments with the WT and Δ*ptsHI* strains were carried out in 96-well plates containing M1 medium and the sugar of interest as the sole carbon source.

Ablation of growth for a carbon source in the Δ*ptsHI* mutant suggests that the sugar is solely PTS transported, whereas a reduction in growth or a reduced growth rate likely indicates import via multiple redundant mechanisms (such as ABC transporters), as well as PTS. Because the area under the curve inherently captures multiple growth parameters, its use is preferable to more commonly used metrics, such as max OD, which may be identical given enough time when comparing strains with significantly different growth rates.

Most metabolizable sugars tested displayed significant growth differences between the wild-type and Δ*ptsHI* mutant, indicating their partial or complete transport via PTS (Fig. 2). PTS-dependent sugars were inferred by comparing the growth (AUC) of the Δ*ptsHI* mutant to that of the no-sugar control. Those within 1 standard deviation, that is, growth in the presence of sugar looks the same as the no-sugar control were deemed to be fully PTS-dependent. PTS-dependent sugars used by *E. faecium* include common dietary sugars, such as sucrose, trehalose, mannitol, maltose, mannose, and lactose (Popkin and Nielsen 2003, Di Rienzi and Britton 2020). Other sugars that are likely to be imported solely via PTS systems include cellobiose, glucosamine, N-acetyl-D-glucosamine, and salacin. Sugars that were marginally outside the no-sugar control range and were potentially transported via multiple mechanisms included arbutin, fructose, and arabinose. Lactulose, maltotriose, and glucose maintained robust growth in the absence of PTS, albeit with a significant reduction compared with the WT. No significant difference in growth was observed when methyl β-d-glucoside (a monosaccharide derived from glucose) or ribose

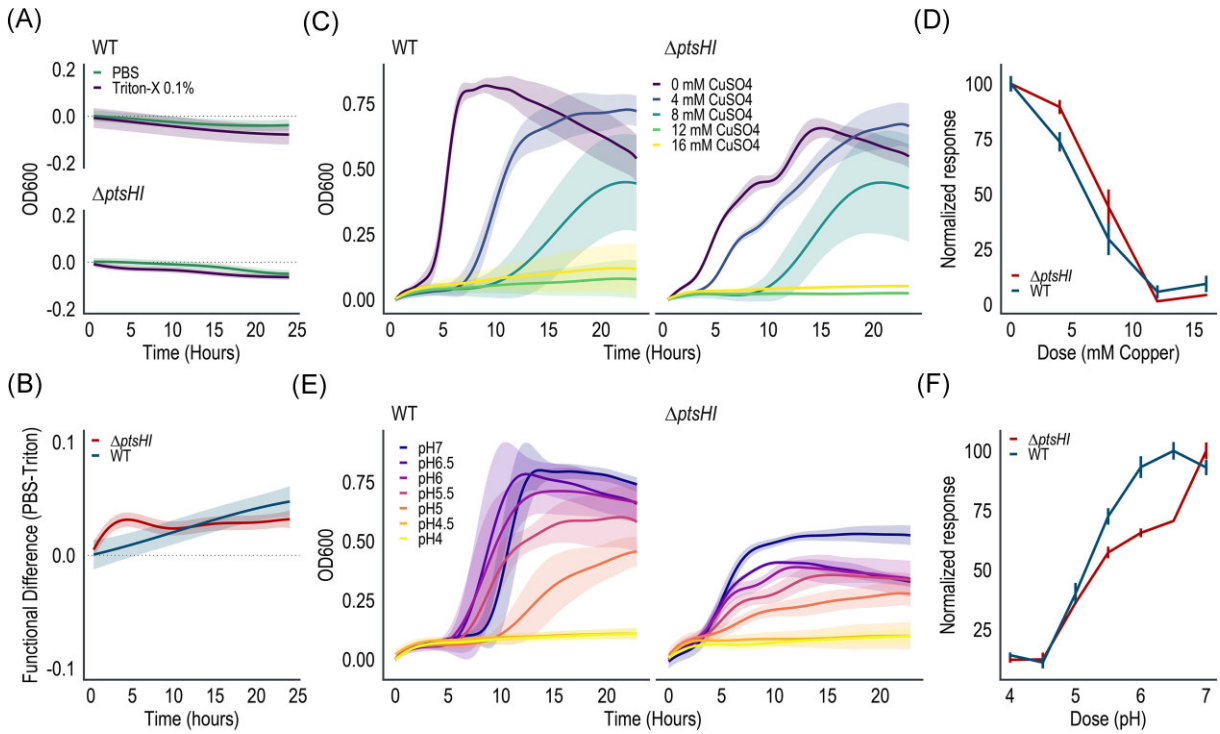

Figure 5. Deletion of *ptsHI* did not affect resistance to multiple stressors. A) Autolysis of the WT and Δ*ptsHI* strains in PBS and 0.1% Triton-X. The solid line indicates the mean drop in OD600, whereas the shaded area represents the 95% CI. Data were calculated from three biological replicates. B) Functional difference (ODΔ = ODHigh − ODLow) in lysis between PBS and PBS + 0.1% Triton-X. The sum of functional differences, ‖ODΔ‖, which quantifies the magnitude of differences between the two curves, was not significantly different between the two strains (mean and 95% confidence interval of 0.355 [0.250,0.459] and 0.330 [0.267,0.392] for the WT and Δ*ptsHI* strains, respectively). C) Growth curves of the WT and Δ*ptsHI* strains with increasing CuSO4 concentrations. D) Dose-response curves for copper concentrations. D) Growth curves of the WT and Δ*ptsHI* strains with decreasing pH. E) Dose-response curves for pH. For C and E, solid lines and shaded areas indicate the mean growth and 95% CI for three biological replicates.

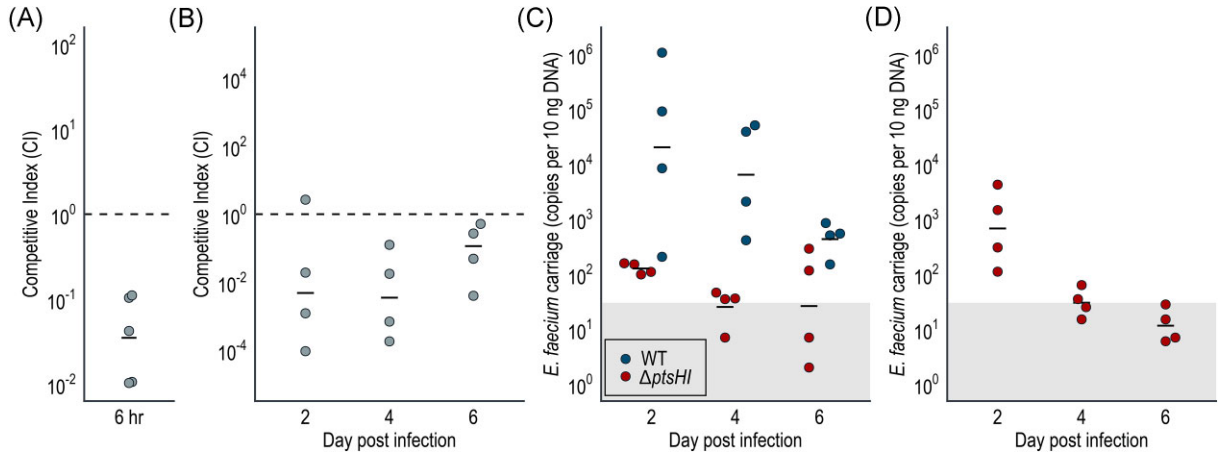

Figure 6. Δ*ptsHI* has a significant competitive disadvantage both *in vitro* and *in vivo*. (A) Competitive index of five separate experiments comparing WT and Δ*ptsHI* strains in BHI media after 6 h. (B) Competitive index over time of the WT vs. Δ*ptsHI* strains in a mouse colonization model. (C) Colonization data used to calculate the competitive index in B. (D) The Δ*ptsHI* strain was rapidly lost from a mouse colonization model when provided as the sole *E. faecium* strain. For C and D, the grey shaded area indicates *E. faecium* copy numbers below the minimum standard of 30 copies.

were used as the sole carbon source. This may mean that PTS are not used to transport these sugars, or that there is a high-affinity, non-PTS system that compensates for the loss of PTS. In low G+C gram-positive bacteria, CcpA, PtsH (HPr), and bifunctional HPr kinase/phosphatase (HPrK/P) are involved in global transcriptional regulation of carbon catabolite repression (CCR) (Grand et al. 2020). The inability to activate CCR due to the absence of PtsH (HPr) in the Δ*ptsHI* mutant could be a confounding factor stemming from its reduced ability to regulate gene expression. Overall, there was robust evidence for the involvement of PTS transporters in 16 of the 18 single carbon sources found to be metabolizable by *E. faecium*.

Growth phenotype of *the E. faecium* Δ*ptsHI* mutant in rich media

To assess how deletion of the *ptsHI* operon affects growth in a nutrient-rich environment, we grew WT, mutant, and complemented strains in brain-heart infusion (BHI) media. The mutant strain showed attenuated growth, with a significantly reduced maximum OD and area under the curve (AUC), which was restored in the complemented strain (Fig. 3A-C). The mutant also exhibited an increased doubling time compared to the WT strain (0.61 ± 0.16 Vs 0.29 ± 0.05 h, $p < 0.001$) due to a significant reduction in its growth rate (1.17 ± 0.25 Vs 2.44 ± 0.43 h^{-1}, $p < 0.001$).

BHI media traditionally contains 0.2% w/v glucose, which is at least partially imported via PTS in many low G+C bacteria. The Δ*ptsHI* mutant showed a modest but significant reduction in growth when glucose was used as the sole carbon source (Fig. 2). This may be due to a reduced ability to import glucose, a fitness burden of unregulated metabolism via CcpA, or both. To determine whether the growth discrepancy between the strains was due to the presence of glucose, we repeated the experiment in the BHI medium without glucose (Fig. 3A-C). Although all strains showed an overall reduction in growth compared to growth in glucose-complemented BHI, the mutant strain exhibited significantly larger growth defects. It is possible that this is due to a non-nutrient-related fitness cost of the gene deletion or the inability to utilize other sugars present in BHI that are wholly PTS-dependent and therefore only available to the WT or complemented strains.

The Δ*ptsHI* mutant is defective in biofilm formation

Biofilms are important factors in the pathogenesis of enterococcal infections. The ability to form biofilms on implanted medical devices, such as catheters, can provide an advantage to bacteria that protects them from antibiotic assault and phagocytosis and enables recurrent infection (Guiton et al. 2010, Ch'ng et al. 2019). Several factors have been implicated in *E. faecium* biofilm formation, including the enterococcal surface protein (Esp) (Heikens et al. 2007), surface adhesin SgrA (Hendrickx et al. 2009), pili PilA and PilB (Sillanpaa et al. 2010), and the catabolite control protein A (CcpA) (Somarajan et al. 2014). Additionally, PtsH and PtsI have been demonstrated to affect biofilm formation in other bacterial species (Houot and Watnick 2008, Houot et al. 2010a,b, Horng et al. 2018). Therefore, we examined whether deletion of *ptsHI* affected biofilm formation in *E. faecium*.

The Δ*ptsHI* mutant showed significantly reduced biofilm formation compared to the WT strain (Fig. 4). This suggests a role for either or both universal *pts* genes in biofilm formation, possibly by phosphorylating or interacting with a key component in the biofilm formation pathway, such as CcpA.

The PTS system of *E. faecium* does not play a significant role in stress response

Bacteria that live in mammalian hosts as commensals or pathogens face a multitude of stresses. Several survival mechanisms have been linked to sugar metabolism or involve PtsI or PtsH. In *Bacillus subtilis*, many stress response genes are regulated by CcpA/PtsH-dependent catabolite repression (Lorca et al. 2005). To examine the role of *ptsHI* in the stress response of *E. faecium*, we selected three divergent responses: resistance to autolysis, copper toxicity, and acid stress.

The major autolysin AtlA is essential for the release of extracellular DNA (eDNA) into the biofilm matrix, contributing to biofilm attachment and stability. Disruption of this autolysin results in increased resistance to Triton X-100 (Paganelli et al. 2013). To determine whether deletion of *ptsHI* affected autolysis, we exposed the early stationary phase WT and Δ*ptsHI* strains to PBS or PBS + 0.1% Triton-X and monitored the optical density (OD_{600}) over time. As shown in Fig. 5A-B, no significant difference was observed between the strains, indicating that the loss of *ptsHI* did not affect resistance to autolysis.

Resistance to Copper toxicity is an important factor for evading the immune system. Copper accumulates at sites of infection, including the gastrointestinal and respiratory tracts, blood, and urine, and its antibacterial toxicity is directly leveraged by phagocytic cells to kill pathogens (Focarelli et al. 2022). Several studies have shown significant changes in carbon source acquisition, central metabolism, and PTS gene expression in the presence of copper, as well as the fixation of mutants in PTS genes during experimental evolutionary studies on copper resistance (Quesille-Villalobos et al. 2019, Boyd et al. 2022, Dao et al. 2023). Copper signaling has also been demonstrated to regulate the DNA-binding activity of CcpA in *Staphylococcus aureus* (Liao et al. 2022), and excess copper in the environment has been shown to increase the catabolic diversity of Gram-positive bacteria (Yang et al. 2022). To determine whether copper toxicity was ameliorated by the PTS system in *E. faecium*, we propagated the WT and Δ*ptsHI* strains in rich media containing 0-16 mM copper ($CuSO_4$) (Fig. 5C). Analysis of the dose-response curves demonstrated no statistical difference in LD50 between the strains under the conditions tested ($p = 0.166$, Fig. 5D).

Bacteria that colonize via the fecal oral route must transit through the low pH condition of the stomach. A deficiency in PtsI leads to significant downregulation of genes encoding enzymes of the TCA cycle and the electron transport chain, which are crucial for ATP synthesis and energy production in bacteria. This shift in metabolism from the TCA cycle to glycolysis and the pentose phosphate pathway (PPP) can be a response to stress, including acid stress, as it reduces electron transfer and ATP synthesis. In *E. coli*, this metabolic shift allows the bacteria to withstand the lethal actions of various stressors, including acidic conditions (Zeng et al. 2022). In *L. monocytogenes*, sugar metabolism, specifically trehalose transport via TreB, has been observed to affect the response to acid stress (Wu et al. 2023), and there is evidence to suggest that PTS systems can sense environmental cues to activate signaling cascades (Gilbreth et al. 2004, Mertins et al. 2007, Liu et al. 2013, Liu et al. 2017, Wu et al. 2023). Inhibition of carbon catabolite repression may affect these metabolic shifts which occur in response to acid stress. To determine the role of PtsHI in acid survival in *E. faecium*, we grew WT and Δ*ptsHI* strains in pH-adjusted rich media ranging from pH7 to pH4 (Fig. 5E). Comparisons of the dose-response curves demonstrated no statistical difference in LD50 between the strains ($P = 0.836$, Fig. 5F).

The *ptsHI* operon plays a crucial role in competitive fitness

The Δ*ptsHI* mutant exhibited limited capacity to utilize exogenous carbon sources. Given its growth phenotype in rich media, we hypothesized that the WT strain would outperform the isogenic mutant under direct competition. To confirm this, we co-cultured exponentially growing mutant and WT strains at a ratio of approximately 10:1 in fresh BHI medium and allowed them to proliferate for 6 h. The cell densities were determined by plating at T0 and T6, and the competitive index was calculated. As anticipated, the WT strain significantly outcompeted the mutant within this brief 6-hour period (Fig. 6A).

While BHI is nutrient-rich, the mammalian GIT presents a markedly different nutrient environment. The ablation of PtsH mediated CCR in the Δ*ptsHI* mutant along with an inability to import PTS dependent sugars, likely places this strain at a significant disadvantage. To assess whether the Δ*ptsHI* strain could colonize the GIT or compete with the isogenic WT strain, we gavaged ICR mice, previously decolonized of native *E. faecium*, with approximately 10^9 NCTC7171Δ*ptsHI* either alone or in an equal mixture with the WT strain. The levels of *E. faecium* were monitored by qPCR using primers specific to either the total *E. faecium* or the mutant strain. Mirroring the *in vitro* experiment, the Δ*ptsHI* strain was outcompeted by the WT strain (Fig. 6B). Intriguingly, by day 6 post-infection, the competitive index seemed to approach equilibrium; however, this was attributed to a decrease in both the WT and mutant strains, a phenomenon previously observed in *E. faecium* colonization assays (Montealegre et al. 2016) (Fig. 6C). Moreover, when monocolonized without competition from other *E. faecium* strains, the Δ*ptsHI* strain rapidly declined below the lowest point on the standard curve (30 copies per 10 ng total DNA) (Fig. 6D).

Conclusions

Enterococci account for approximately 10% of hospital-associated bacteremia cases and are emerging as primary contributors to sepsis in North America and Europe (Pinholt et al. 2014). Within this context, *E. faecium* constitutes 40% of medically relevant enterococcal bacteremia infections. Understanding the factors involved in successful growth and intestinal colonization of clinical *E. faecium* is crucial for the development of novel treatment strategies. Reducing the bacterial burden in the gut decreases the likelihood of translocation to the bloodstream, where it may establish an invasive infection (Weinstock et al. 2007, Taur et al. 2012, Archambaud et al. 2019). Therefore, a mechanism that can achieve this goal may be beneficial.

Targeting the universal PTS enzymes PtsI and PtsH has a range of negative effects on *E. faecium*. The Δ*ptsHI* mutant exhibited impaired growth in nutrient-rich media, diminished biofilm formation, and a decrease in competitive fitness under both *in vitro* and *in vivo* conditions compared with the WT strain. The absence of *ptsHI* puts *E. faecium* at a disadvantage due to its incapacity to transport PTS-dependent sugars and its inability to regulate genes via PtsH mediated carbon catabolite repression. This disadvantage is further amplified by a reduced capacity to form biofilms. Although not investigated in this study, biofilms serve as a critical defense mechanism against phagocytosis and antibiotics, as well as acting as a reservoir for recurrent infection. Consequently, this inhibition may facilitate clearance of infection via other means. Overall, PtsI and PtsH have crucial roles beyond sugar metabolism and significantly contribute to the competitive fitness of *E. faecium* in a variety of ways.

Transport of sugars via the PTS is dominant in *E. faecium* and highlights the need for further studies in the context of intestinal colonization and bloodstream infection. The reliance on PTS systems may provide an opportunity to leverage this trait against highly antibiotic-resistant bacteria. Targeting universal PtsI and H proteins could reduce the ability of *E. faecium* to compete with other microbes. However, the conserved nature of these genes would likely lead to a broad-spectrum approach, which may be undesirable. The identification and targeting of specific PTS systems may offer a more targeted approach. Zhang et al. (2013) identified a unique phosphotransferase system that allows for the utilization of amino sugars, which occur on epithelial cell surfaces, and mucin. The deletion of this PTS significantly reduced the competitive fitness of this mutant in the antibiotic-perturbed GI tract.

Finally, it may be possible to use the sugar phosphates generated when PTS imports sugars from the environment as a novel therapeutic strategy. Toxicity resulting from the accumulation of sugar-phosphate molecules is an evolutionarily conserved phenomenon observed in multiple bacterial and eukaryotic systems. Five sugar-phosphate toxicities are thought to be specific to bacteria (arabinose [araD], rhamnose [rhaD], fructose-asparagine [fraB], maltose [glgE], and fructose [fruK]), whereas trehalose [ostB] via Tre-6P sugar-phosphate toxicity occurs in fungal pathogens and bacteria but not in humans, rendering them ideal therapeutic targets (Boulanger et al. 2021). Further work is needed to identify the specificity of individual transporters and the role they play in invasion and colonization and to examine the possibility of leveraging these systems as novel treatment mechanisms.

Acknowledgments

This work was supported in part by a grant from the Jewish Heritage Fund for Excellence Research Recruitment Grant Program at the University of Louisville, School of Medicine, and Centers of Biomedical Research Excellence (CoBRE) Grant P20GM125504.

Author contributions

Michelle Hallenbeck, Michelle Chua, and James Collins

Supplementary data

Supplementary data is available at *FEMSMC Journal* online.

Conflict of interest: None declared.

References

Archambaud C, Derre-Bobillot A, Lapaque N *et al.* Intestinal translocation of enterococci requires a threshold level of enterococcal overgrowth in the lumen. *Sci Rep* 2019;**9**:8926.

Beaufils S, Sauvageot N, Maze A *et al.* The cold shock response of Lactobacillus casei: relation between HPr phosphorylation and resistance to freeze/thaw cycles. *J Mol Microbiol Biotechnol* 2007;**13**:65–75.

Bier N, Hammerstrom TG, Koehler TM. Influence of the phosphoenolpyruvate:carbohydrate phosphotransferase system on toxin gene expression and virulence in Bacillus anthracis. *Mol Microbiol* 2020;**113**:237–52.

Boulanger EF, Sabag-Daigle A, Thirugnanasambantham P *et al.* Sugar-phosphate toxicities. *Microbiol Mol Biol Rev* 2021;**85**:e0012321.

Boyd SM, Rhinehardt KL, Ewunkem AJ *et al.* Experimental evolution of copper resistance in Escherichia coli produces evolutionary trade-offs in the antibiotics chloramphenicol, bacitracin, and sulfonamide. *Antibiotics (Basel)* 2022;**11**:711.

Ch'ng JH, Chong KKL, Lam LN *et al.* Biofilm-associated infection by enterococci. *Nat Rev Micro* 2019;**17**:82–94.

Chua MJ, Collins J. Rapid, efficient, and cost-effective gene editing of Enterococcus faecium with CRISPR-Cas12a. *Microbiol Spectr* 2022;**10**:e0242721.

Dao TH, Iverson A, Neville SL *et al.* The role of CopA in Streptococcus pyogenes copper homeostasis and virulence. *J Inorg Biochem* 2023;**240**:112122.

Derkaoui M, Antunes A, Poncet S *et al.* The phosphocarrier protein HPr of Neisseria meningitidis interacts with the transcription regulator CrgA and its deletion affects capsule production, cell adhesion, and virulence. *Mol Microbiol* 2016;**100**:788–807.

Deutscher J, Francke C, Postma PW. How phosphotransferase system-related protein phosphorylation regulates carbohydrate metabolism in bacteria. *Microbiol Mol Biol Rev* 2006;**70**:939–1031.

Di Rienzi SC, Britton RA. Adaptation of the gut microbiota to modern dietary sugars and sweeteners. *Adv Nutr* 2020;**11**:616–29.

Fajstova A, Galanova N, Coufal S *et al.* Diet rich in simple sugars promotes pro-inflammatory response via gut microbiota alteration and TLR4 signaling. *Cells* 2020;**9**:2701.

Fiore E, Van Tyne D, Gilmore MS *et al.* Pathogenicity of enterococci. *Microbiol Spectr* 2019;**7**.

Focarelli F, Giachino A, Waldron KJ. Copper microenvironments in the human body define patterns of copper adaptation in pathogenic bacteria. *PLoS Pathog* 2022;**18**:e1010617.

Galinier A, Deutscher J. Sophisticated regulation of transcriptional factors by the bacterial phosphoenolpyruvate: sugar phosphotransferase system. *J Mol Biol* 2017;**429**:773–89.

Gao W, Howden BP, Stinear TP. Evolution of virulence in Enterococcus faecium, a hospital-adapted opportunistic pathogen. *Curr Opin Microbiol* 2018;**41**:76–82.

Gera K, Le T, Jamin R *et al.* The phosphoenolpyruvate phosphotransferase system in group A Streptococcus acts to reduce streptolysin S activity and lesion severity during soft tissue infection. *Infect Immun* 2014;**82**:1192–204.

Gilbreth SE, Benson AK, Hutkins RW. Catabolite repression and virulence gene expression in Listeria monocytogenes. *Curr Microbiol* 2004;**49**:95–98.

Gilmore MS, Lebreton F, van Schaik W. Genomic transition of enterococci from gut commensals to leading causes of multidrug-resistant hospital infection in the antibiotic era. *Curr Opin Microbiol* 2013;**16**:10–16.

Grand M, Riboulet-Bisson E, Deutscher J *et al.* Enterococcus faecalis maltodextrin gene regulation by combined action of maltose gene regulator MalR and pleiotropic regulator CcpA. *Appl Environ Microb* 2020;**86**:e01147–20.

Graumann P, Schroder K, Schmid R *et al.* Cold shock stress-induced proteins in Bacillus subtilis. *J Bacteriol* 1996;**178**:4611–9.

Guiton PS, Hung CS, Hancock LE *et al.* Enterococcal biofilm formation and virulence in an optimized murine model of foreign body-associated urinary tract infections. *Infect Immun* 2010;**78**:4166–75.

Heikens E, Bonten MJ, Willems RJ. Enterococcal surface protein esp is important for biofilm formation of Enterococcus faecium E1162. *J Bacteriol* 2007;**189**:8233–40.

Hendrickx AP, van Luit-Asbroek M, Schapendonk CM *et al.* SgrA, a nidogen-binding LPXTG surface adhesin implicated in biofilm formation, and EcbA, a collagen binding MSCRAMM, are two novel adhesins of hospital-acquired Enterococcus faecium. *Infect Immun* 2009;**77**:5097–106.

Holm S. A simple sequentially rejective multiple test procedure. *Scand J Stat* 1979;**6**:65–70.

Horng YT, Wang CJ, Chung WT *et al.* Phosphoenolpyruvate phosphotransferase system components positively regulate Klebsiella biofilm formation. *J Microbiol Immunol Infect* 2018;**51**:174–83.

Houot L, Chang S, Absalon C *et al.* Vibrio cholerae phosphoenolpyruvate phosphotransferase system control of carbohydrate transport, biofilm formation, and colonization of the germfree mouse intestine. *Infect Immun* 2010a;**78**:1482–94.

Houot L, Chang S, Pickering BS *et al.* The phosphoenolpyruvate phosphotransferase system regulates vibrio cholerae biofilm formation through multiple independent pathways. *J Bacteriol* 2010b;**192**:3055–67.

Houot L, Watnick PI. A novel role for enzyme I of the Vibrio cholerae phosphoenolpyruvate phosphotransferase system in regulation of growth in a biofilm. *J Bacteriol* 2008;**190**:311–20.

Khan S, Waliullah S, Godfrey V *et al.* Dietary simple sugars alter microbial ecology in the gut and promote colitis in mice. *Sci Transl Med* 2020;**12**:eaay6218.

Kim E, Kim D-S, Yang S-M *et al.* The accurate identification and quantification of six Enterococcus species using quantitative polymerase chain reaction based novel DNA markers. *LWT* 2022;**166**:113769.

Kok M, Bron G, Erni B *et al.* Effect of enzyme I of the bacterial phosphoenolpyruvate : sugar phosphotransferase system (PTS) on virulence in a murine model. *Microbiology (Reading)* 2003;**149**:2645–52.

Le Bouguenec C, Schouler C. Sugar metabolism, an additional virulence factor in enterobacteria. *Int J Med Microbiol* 2011;**301**:1–6.

Lebreton F, van Schaik W, McGuire AM *et al.* Emergence of epidemic multidrug-resistant Enterococcus faecium from animal and commensal strains. *mBio* 2013;**4**:e00534–13.

Lebreton F, van Schaik W, Sanguinetti M *et al.* AsrR is an oxidative stress sensing regulator modulating Enterococcus faecium opportunistic traits, antimicrobial resistance, and pathogenicity. *PLoS Pathog* 2012;**8**:e1002834.

Liao X, Li H, Guo Y *et al.* Regulation of DNA-binding activity of the Staphylococcus aureus catabolite control protein A by copper (II)-mediated oxidation. *J Biol Chem* 2022;**298**:101587.

Liu Y, Ceruso M, Jiang Y *et al.* Construction of Listeria monocytogenes mutants with in-frame deletions in the phosphotransferase transport system (PTS) and analysis of their growth under stress conditions. *J Food Sci* 2013;**78**:M1392–1398.

Liu Y, Yoo BB, Hwang CA *et al.* LMOf2365_0442 Encoding for a fructose specific PTS permease IIA may Be required for virulence in L. monocytogenes strain F2365. *Front Microbiol* 2017;**8**:1611.

Lorca GL, Chung YJ, Barabote RD *et al.* Catabolite repression and activation in Bacillus subtilis: dependency on CcpA, HPr, and HprK. *J Bacteriol* 2005;**187**:7826–39.

Menghani SV, Cutcliffe MP, Sanchez-Rosario Y *et al.* N,N-dimethyldithiocarbamate elicits pneumococcal hypersensitivity to copper and macrophage-mediated clearance. *Infect Immun* 2022;**90**:e0059721.

Mertins S, Joseph B, Goetz M *et al.* Interference of components of the phosphoenolpyruvate phosphotransferase system with the central virulence gene regulator PrfA of Listeria monocytogenes. *J Bacteriol* 2007;**189**:473–90.

Midani FS, Collins J, Britton RA. AMiGA: software for automated analysis of microbial growth assays. *Msystems* 2021;**6**:e0050821.

Min H, Seok YJ. Phosphotransferase system sugars immediately induce mutations of Cra in an Escherichia coli ptsH mutant. *Environ Microbiol* 2022;**24**:5425–36.

Monedero V, Maze A, Boel G *et al.* The phosphotransferase system of Lactobacillus casei: regulation of carbon metabolism and connection to cold shock response. *J Mol Microbiol Biotechnol* 2007;**12**:20–32.

Montealegre MC, Singh KV, Murray BE. Gastrointestinal tract colonization dynamics by different Enterococcus faecium clades. *J Infect Dis* 2016;**213**:1914–22.

Paganelli FL, Huebner J, Singh KV *et al.* Genome-wide screening identifies phosphotransferase system permease BepA to Be involved

in Enterococcus faecium endocarditis and biofilm formation. *J Infect Dis* 2016;**214**:189–95.
Paganelli FL, Willems RJ, Jansen P *et al.* Enterococcus faecium biofilm formation: identification of major autolysin AtlAEfm, associated Acm surface localization, and AtlAEfm-independent extracellular DNA release. *mBio* 2013;**4**:e00154.
Peng Z, Ehrmann MA, Waldhuber A *et al.* Phosphotransferase systems in Enterococcus faecalis OG1RF enhance anti-stress capacity in vitro and in vivo. *Res Microbiol* 2017;**168**:558–66.
Phadtare S. Recent developments in bacterial cold-shock response. *Curr Iss Mol Biol* 2004;**6**:125–36.
Pinholt M, Ostergaard C, Arpi M *et al.* Incidence, clinical characteristics and 30-day mortality of enterococcal bacteraemia in Denmark 2006-2009: a population-based cohort study. *Clin Microbiol Infect* 2014;**20**:145–51.
Popkin BM, Nielsen SJ. The sweetening of the world's diet. *Obes Res* 2003;**11**:1325–32.
Quesille-Villalobos AM, Parra A, Maza F *et al.* The combined effect of cold and copper stresses on the proliferation and transcriptional response of Listeria monocytogenes. *Front Microbiol* 2019;**10**:612.
Ritz C, Baty F, Streibig JC *et al.* Dose-response analysis using R. *PLoS One* 2015;**10**:e0146021.
Sillanpaa J, Nallapareddy SR, Singh KV *et al.* Characterization of the ebp(fm) pilus-encoding operon of Enterococcus faecium and its role in biofilm formation and virulence in a murine model of urinary tract infection. *Virulence* 2010;**1**:236–46.
Somarajan SR, Roh JH, Singh KV *et al.* CcpA is important for growth and virulence of Enterococcus faecium. *Infect Immun* 2014;**82**:3580–7.
Starikova I, Al-Haroni M, Werner G *et al.* Fitness costs of various mobile genetic elements in Enterococcus faecium and Enterococcus faecalis. *J Antimicrob Chemother* 2013;**68**:2755–65.
Stein-Thoeringer CK, Nichols KB, Lazrak A *et al.* Lactose drives Enterococcus expansion to promote graft-versus-host disease. *Science* 2019;**366**:1143–9.
Taur Y, Xavier JB, Lipuma L *et al.* Intestinal domination and the risk of bacteremia in patients undergoing allogeneic hematopoietic stem cell transplantation. *Clin Infect Dis* 2012;**55**:905–14.
Turner AM, Lee JYH, Gorrie CL *et al.* Genomic insights into last-line antimicrobial resistance in multidrug-resistant *Staphylococcus* and vancomycin-resistant *Enterococcus*. *Front Microbiol* 2021;**12**:637656.
Wang Y, Qi W, Song G *et al.* High-fructose diet increases inflammatory cytokines and alters gut microbiota composition in rats. *Mediat Inflamm* 2020;**2020**:6672636.
Weinstock DM, Conlon M, Iovino C *et al.* Colonization, bloodstream infection, and mortality caused by vancomycin-resistant Enterococcus early after allogeneic hematopoietic stem cell transplant. *Biol Blood Marrow Transplant* 2007;**13**:615–21.
Wickham H, Averick M, Bryan J *et al.* Welcome to the Tidyverse. *J Open Source Software* 2019;**4**:1686.
Wu J, McAuliffe O, O'Byrne CP. Trehalose transport occurs via TreB in Listeria monocytogenes and it influences biofilm development and acid resistance. *Int J Food Microbiol* 2023;**394**:110165.
Yang M, Liu Y, Liao Y *et al.* Excess copper promotes catabolic activity of gram-positive bacteria and resistance of gram-negative bacteria but inhibits fungal community in soil. *Environ Sci Pollut Res Int* 2022;**29**:22602–12.
Zeng J, Hong Y, Zhao N *et al.* A broadly applicable, stress-mediated bacterial death pathway regulated by the phosphotransferase system (PTS) and the cAMP-crp cascade. *Proc Natl Acad Sci USA* 2022;**119**:e2118566119.
Zhang X, Top J, de Been M *et al.* Identification of a genetic determinant in clinical Enterococcus faecium strains that contributes to intestinal colonization during antibiotic treatment. *J Infect Dis* 2013;**207**:1780–6.
Zhang X, Vrijenhoek JE, Bonten MJ *et al.* A genetic element present on megaplasmids allows Enterococcus faecium to use raffinose as carbon source. *Environ Microbiol* 2011;**13**:518–28.

Received 13 March 2024; **revised** 8 May 2024; **accepted** 31 May 2024